ORIGINAL ARTICLE

Investigation on microstructure and mechanical properties of double-sided synchronous TIP TIG arc butt welded duplex stainless steel

Lulu Wang[1] · Pengcheng Zhao[1] · Jiajing Pan[1] · Long Tan[1] · Kaixing Zhu[1]

Abstract

Double-sided synchronous TIP TIG arc butt welding (DSSTTABW) is firstly carried out to join 5-mm SAF 2205 duplex stainless steel (DSS) plates without grooving. The microstructure and mechanical properties of DSSTTABW joints, including microhardness, transverse tension, and bend properties, are evaluated systematically. Results show that sound DSS joint, with excellent appearance and properties, can be obtained through the DSSTTABW process. In DSSTTABW joints, a deal of second austenite ($\gamma2$) appears in the weld metal, resulting in a slight increment of austenite volume fraction of the weld zone. Meanwhile sigma (σ) phase precipitates at the grain boundaries of delta ferrite (δ-Fe) and austenite of the weld zone. Mechanical property tests show that the DSSTTABW weldment exhibits higher tensile strength and microhardness but lower ductility compared to 2205 DSS base metal due to the existing Widmänstten-type austenite (WA) and σ phase. All weldments fracture at the weld zones in the mode of ductile. After bending tests, no surface cracks are observed on the DSSTTABW joint.

Keywords Double-sided synchronous TIP TIG arc butt welding (DSSTTABW) · 2205 duplex stainless steel · Mechanical properties

1 Introduction

Duplex stainless steel (DSS) is more and more preferably applied in the fabrication of ocean engineering and pipes to petrochemical and pressure vessels due to its advantages of combining good corrosion resistance with high strength. The excellent properties of DSS depend on appropriate austenite/ferrite phase proportion, which is preferably expected to be 1:1. Nevertheless, the austenite/ferrite volume fraction tends to deviate from 1:1 during the welding process, in either the weld metal (WM) or the heat-affected zone (HAZ), which considerably influences mechanical properties and corrosion resistance.

Some investigations have been devoted to the welding of 2205 DSS; almost all of the welding methods have been successfully applied in the joining of 2205 DSS. Wang et al. [1] compared the microstructure and properties of an 8-mm-thick dissimilar joint welded by gas tungsten inert welding (GTAW) and shielded metal arc welding (SMAW). Their research indicated that the 2205 DSS joint welded by both GTAW and SMAW could obtain satisfactory mechanical properties, while the GTAW joint got better corrosion resistance than the SMAW joint. They pointed out that GTAW is more suitable for the dissimilar joining of 2205 DSS and 16MnR. Chern et al. [2] analyzed the effects of kinds of fluxes on the activated tungsten inert gas (A-TIG) welding joint. They indicated that the A-TIG welded joint has better mechanical properties, larger penetration, and smaller distortion, but with higher heat input than the traditional tungsten inert welding (TIG) joint. Westin et al. [3] successfully adopted a laser-GMA hybrid welding technique to join 13.5-mm DSS in a single pass. They illustrated that the laser-GMA hybrid welding joint has higher ferrite/austenite ratio due to the high welding speed and cooling rate, which severely reduces the corrosion resistance and ductility of welding joints. Esmailzadeh et al. [4] investigated the influences of different welding speeds on the microstructure and mechanical

✉ Lulu Wang
   wanglulu@qust.edu.cn

1   College of Electromechanical Engineering, Qingdao University of Science and Technology, QingdaoShandong Province, People's Republic of China

Fig. 1 **a** Schematic of the DSSTTABW process. **b** Assembly of the DSSTTABW process
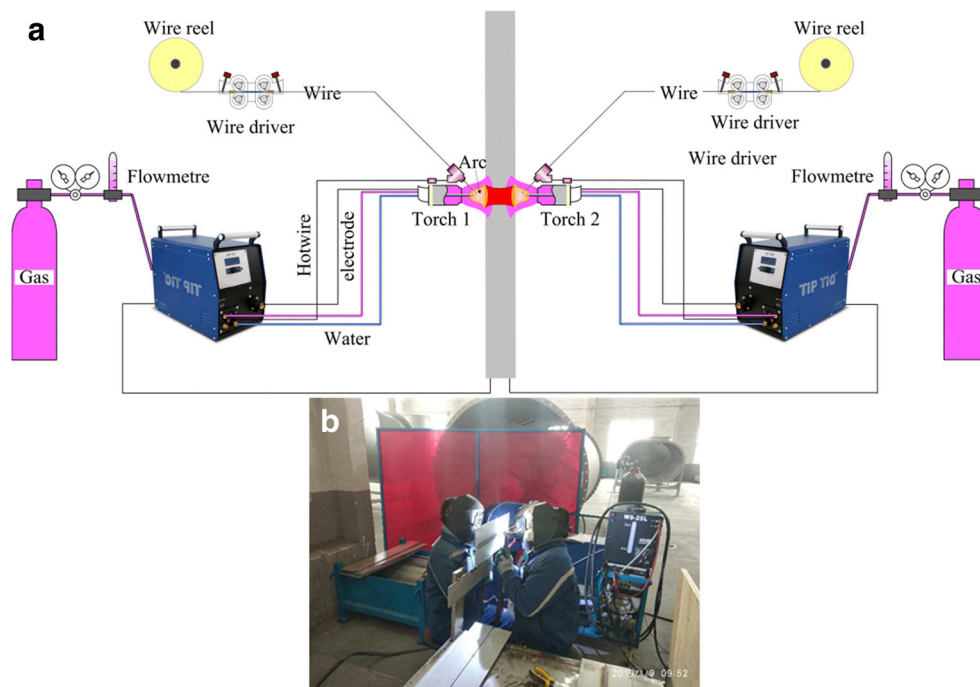
properties during friction stir welding (FSW) and demonstrated that lower heat input is the key in obtaining higher quality joints. The variation of second phase and its effects on mechanical properties of the submerged arc welded (SAW) joint during post weld heat treatment (PWHT) were presented in the research of Luo et al. [5]. The results showed that PWHT could decrease the amount of second phase in the SAW joint and thus improving the mechanical properties. Geng et al. [6] successfully joined the 2205 DSS by using double-pass gas tungsten inert welding, and systematically analyzed the microstructure and corrosion resistance of the GTAW joint. They pointed out that lots of second austenite ($\gamma2$) appeared in WM and pitting corrosion resistance of the fusion line of the GTAW joint is the worst. Hosseini et al. studied the effects of heat input and weld pass during tungsten inert welding (TIG) on microstructure [7] and corrosion resistance [8]. It can be concluded that less welding pass with higher heat input led to less second phase and higher corrosion resistance. Selva et al. [9] joined 2205 DSS by using the plasma arc welding (PAW) method, and optimized the welding parameters. Although all welding processes mentioned above have been successfully applied in joining the 2205 DSS, the higher heat input during

welding leads to higher ferrite/austenite ratio in weld, which severely reduces the joint's mechanical properties. All the references mentioned above illustrated that heat input is key in obtaining high-quality DSS joints.

Double-sided arc welding (DSAW) is a novel welding process devised by Zhang et al. [10] to improve the properties of the aluminum welding joint, which combines two GTAW torches on each side of the workpiece synchronously, resulting in a large reduction in heat input. Zhao et al. [11] applied the arc and laser synchronously in the welding of 6-mm aluminum alloy and indicated that laser-arc double-sided welding (LADSW) is a better choice for joining of aluminum alloy compared to DSAW. Wei et al. [12] joined the aluminum alloy by using two GTA torches coaxially and investigated the angular deformation and mechanical properties. Peng et al. applied the DSAW in the welding of steel, and analyzed the influence of thermal cycle on the microstructure and properties of HAZ [13, 14] and weld toe [15] of welding joints. Zheng et al. [16–18] successfully introduced the MIG-TIG DSAW technique to forming Al-steel dissimilar welding joints, illustrating that the DSAW technique obviously decreased the heat input and then obtained sound welding joint.

Table 1 Technological parameters used in the DSSTTABW process

	Current (A)	Voltage (V)	Welding speed (mm/min)	Wire feed speed (m/min)	Heat input (kJ/mm)	Heater current (A)	Gas flow (L/min)
Side 1	100	14	170	25	0.34	70	25
Side 2	100	14	170	25	0.34	70	25

Table 2 Chemical composition (wt%) and mechanical properties of 2205 DSS and ER2209

	C	Si	Mn	P	S	Cr	Ni	Mo	Nb	Cu	Co	N	Fe	Rp0.2 (MPa)	Rm (MPa)	A5 (%)
2205	0.018	0.39	1.35	0.019	0.001	22.45	5.74	3.18	0.011	0.34	0.160	0.171	Bal.	500	700 (Min)	25
ER2209	0.01	0.4	1.7	0.01	0.01	22.5	8.6	3.1	-	0.1	-	0.15	Bal.	600	770 (Min)	27

Wang et al. [19] successfully joined the high-nitrogen austenitic stainless steel by DSAW. All the references indicated that DSAW could reduce the heat input and thus improve the properties of welding joints.

TIP TIG is another novel type of semi-automatic tungsten inert gas (TIG) welding process, proposed by Madsen at Aalborg University in 2007 [20]. During the TIP TIG welding process, the wire is preheated and oscillated. The TIP TIG welding process advances in heat input controlling by guiding the preheated and oscillating filler wire directly into the weld pool [21]. To date, few researches were available for TIP TIG welding.

In this paper, double-sided synchronous TIP TIG arc butt welding (DSSTTABW) is firstly applied to joining 2205 DSSs without any groove. After welding, appearance, microstructure, and mechanical properties of the welding joints formed by the method were investigated.

2 Experimental procedures

Figure 1 shows the schematic of the DSSTTABW system. Two TIP TIG torches controlled by two handlers were laid on each side of the 2205 DSS plate symmetrically, while the 2205 DSS plates are assembled horizontally by tacking on the welding platform. During the

DSSTTABW process, two TIP TIG torches were synchronously moved from the same starting point at the same speed during the welding process to form a single weld pool, and both torches were perpendicular to the plate surface. Cerium-tungsten (WC 20) with a diameter of 3.2 mm is used as the electrode, which is shielded by pure argon during the welding process. The optimized welding parameters are listed in Table 1.

DSSTTABW is carried out on a 5-mm-thick SAF 2205 DSS plate by using ER2209 as the filler metal. The 2205 DSS plate was cold rolled and then annealed at 1100 °C for 30 min in argon flow. The composition and mechanical properties of SAF 2205 DSS and ER2209 are summarized in Table 2. Before welding, 25 mm from either side of the bevel was polished with 400 grit silicon carbide paper and cleaned subsequently with isopropyl alcohol to confirm that the base metal surface is free from contamination. The two 2205 DSS plates without a groove were assembled with a gap of 2 mm by tacking, and then they were butt-welded.

After welding, macro- and microstructure characterization investigation and mechanical property analysis of DSSTTABW joints, including tensile, hardness, and bend test, are carried out. The microstructure samples were etched by aqua regia (30 ml HNO_3 + 10 ml HCL) for 15 s, and then analyzed by optical microscopy (OM), scanning electron
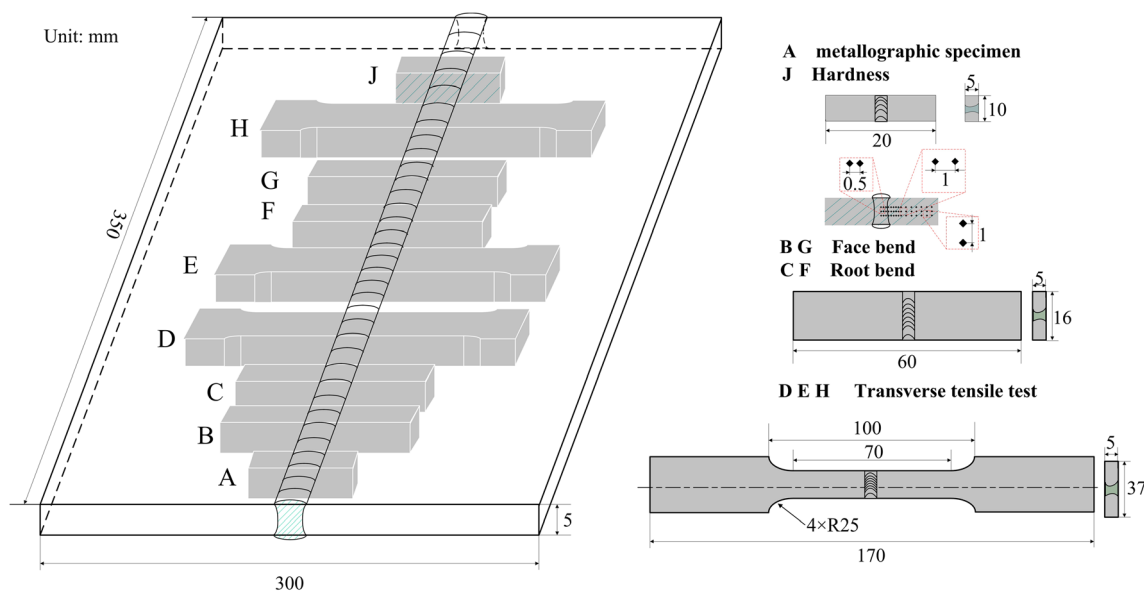
Fig. 2 Location of samples in the DSSTTABW joint used for the transverse tensile test, bend test, and metallographic and hardness examination

Fig. 3 Appearance and cross section of DSSTTABW arc butt welding for 2205 (W_m is the minimum width of weld, W_f is the weld width of front side, W_r is the weld width of back side). **a** Front side. **b** Back side. **c** The joint cross section
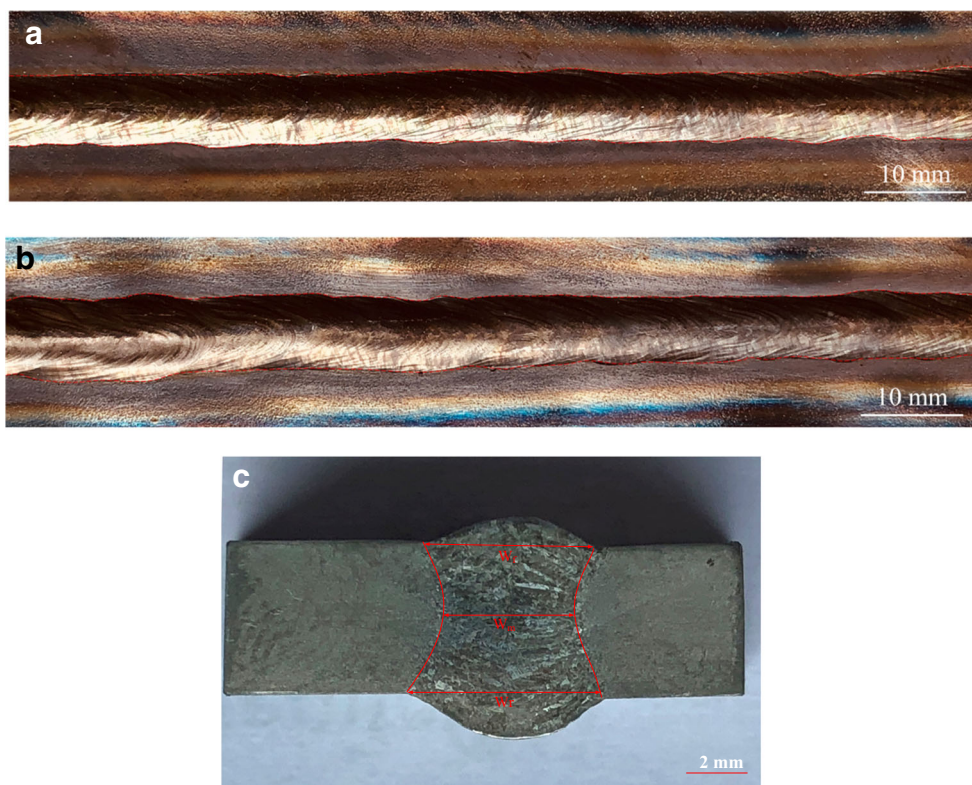
microscopy (SEM), and energy-dispersive X-ray spectroscopy (EDS). The ferrite content is investigated by using the FERITSCOPE FMP30 based on the magnetic conductivity principle. Vickers microhardness tests were performed on polished samples. Tensile and bend tests are carried out according to ISO 4136 [22] and ISO 5173 [23], respectively.
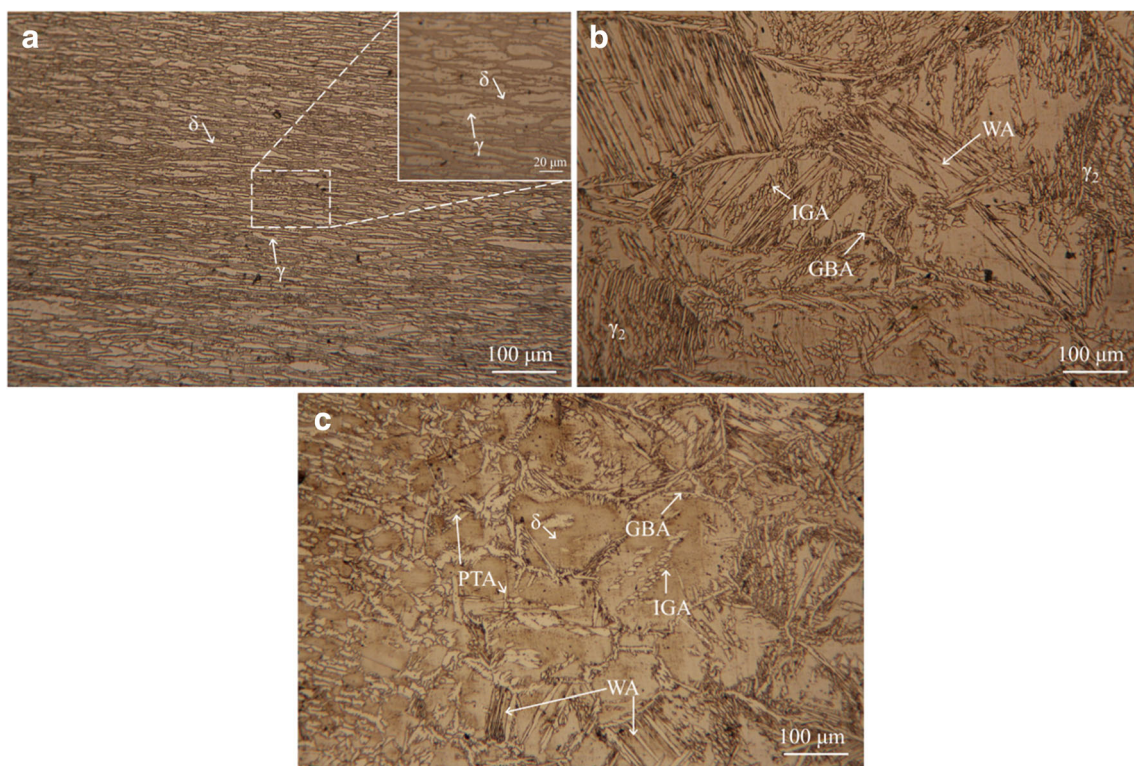
Fig. 4 Optical micrograph of DSSTTABW joint. **a** BM. **b** WM. **c** Transition zone

Fig. 5 SEM morphologies of various microstructural zones of the DSSTTABW joint. **a** BM. **b** HAZ. **c** WM. **d** The enlargement of the square zone in (**c**)
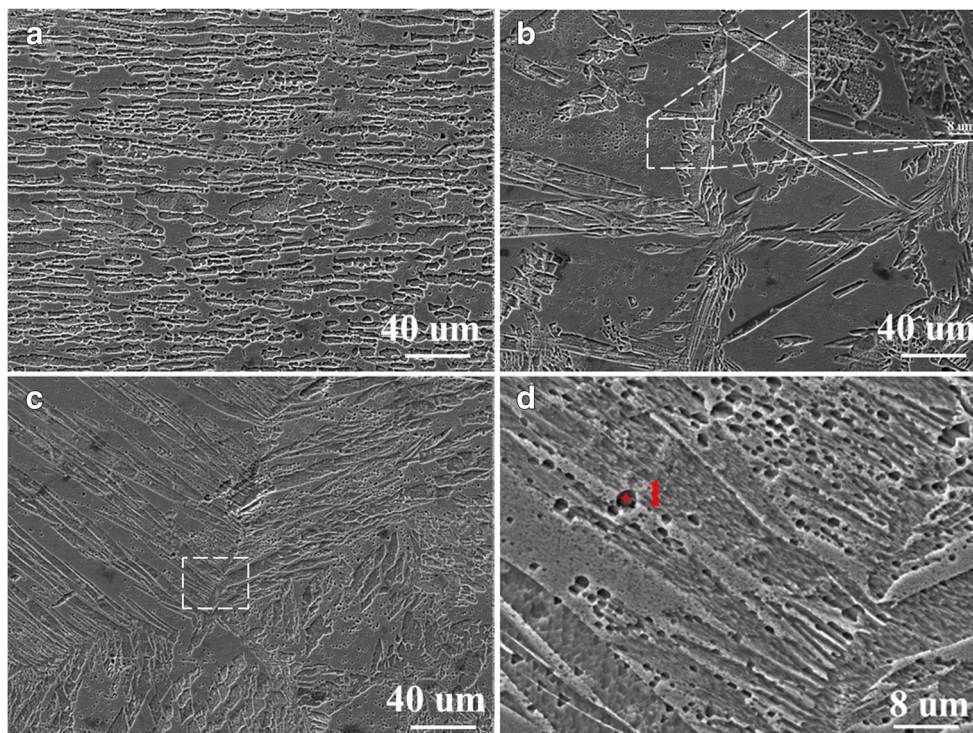
The specimens are prepared in the dimension as shown in Fig. 2. The fracture morphology of tensile specimens is investigated by using SEM equipped with EDS.

3 Results and discussion

3.1 Appearance and macrostructure

Figure 3a and b exhibit the front and back appearance welded by DSSTTABW, respectively. It can be found that a uniform weld seam without any surface defect can be realized on the two sides of the welding joint. Figure 3c shows the cross section and the weld width definitions of the DSSTTABW joint. The quantities of the front and back molten metal are basically identical. The weld width of front side W_f is 6 mm, the width of back side W_r is 7 mm, and the minimum weld width W_m is 4.35 mm, located at the weld center.

3.2 Microstructure and austenite volume fraction

Figure 4 presents the optical micrograph of the DSSTTABW joint. As shown in Fig. 4a, the 2205 DSS base metal consists of stripe-type austenite phase (γ, light color) and continuous ferrite phase matrix (δ-Fe, dark color). The weld metal (WM) of the DSSTTABW joint is comprised of δ-Fe and four types of austenite phase, including grain boundary austenite (GBA), intragranular austenite (IGA),

Widmänstten-type austenite (WA), and secondary austenite ($\gamma2$). Due to the higher grain boundary energy, the GBA is initially nucleated at the boundaries of δ-Fe grain, and subsequently the WA forms and grows inward into the δ-Fe grain. Meanwhile, lots of IGA appear in the ferrite grains. The formation of IGA can be attributed to the fact that the filler wire 2209 bright higher content of nickel into weld. Moreover, the dissolution of nitrides in WM leads to the formation of more $\gamma2$ [24]. Figure 4c illustrates the optical microstructure of the transition region from the WM to base metal (BM), which can be divided into three parts. The left part of the transition zone is similar with the base metal (Fig. 4a), while the right part has a similar microstructure with the weld zone (Fig. 4b). The middle part of the transition zone is the HAZ, consisting of δ-Fe, GBA, WA, IGA, and partially transformed austenite (PTA).

The SEM micrographs of the DSSTTABW joint are conducted and shown in Fig. 5. The microstructure of HAZ and WM contains δ-Fe, lath WA, and block austenite. The block austenite arranges regularly along the growth direction of WA. And a cluster of intergranular austenite forms in the δ-

Table 3 Composition measurements by EDS at point 1 in Fig. 5 (wt%)

	Fe	Cr	Ni	Mo	C	Mn	Si
μ	52.3	32.38	7.11	3.9	2.72	1.29	0.3
s	1.49	0.55	0.2	0.12	0.42	0.06	0.04

μ is the average value, s is the standard deviation
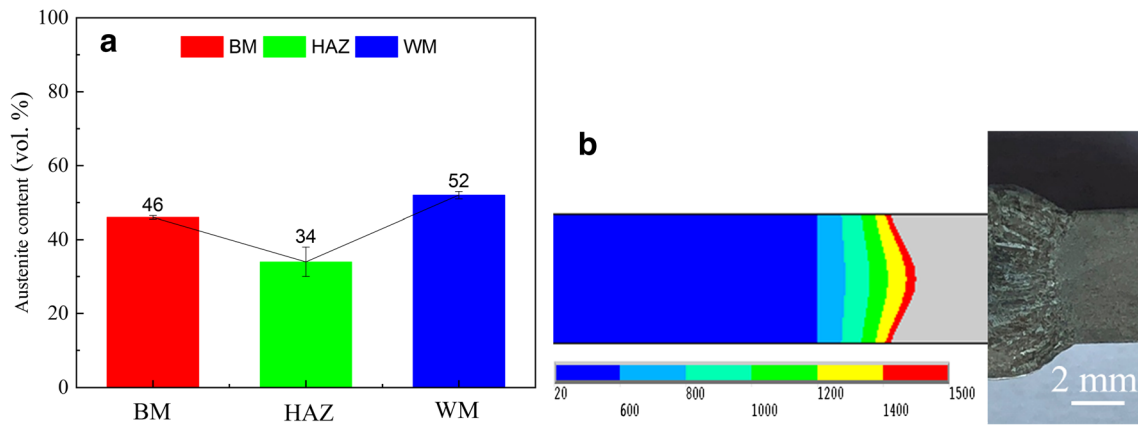
Fig. 6 **a** Austenite contents in various microstructural zones of the DSSTTABW joint. **b** The temperature distribution during the DSSTTABW process calculated by ANSYS

Fe matrix. Second phases in the average size of 2 μm precipitate at the grain boundaries of δ-Fe and austenite of the weld zone. The EDS result, summarized in Table 3, indicates that the second phase is sigma (σ) phase, which contains higher volumes of elements Cr and Mo. The existing σ may decrease the ductility of the DSSTTABW joint.

The austenite contents in different zones of the DSSTTABW joint shown in Fig. 6 are measured by using the FERITSCOPE FMP30. The high-quality joint calls for appropriate phase balance, which is higher than 30% austenite in the DSS welding joint [25]. The austenite proportion in the weld zone of the DSSTTABW joint is 52%, which is slightly higher than the original material (46%). It can be attributed to that the adoptive wire ER2209 during the DSSTTABW process contains higher Ni than the 2205 DDS. The austenite content in HAZ is 34%, which is much less than that of BM. The

phase balance in HAZ is the original wrought plate plus an additional thermal cycle, and high quench temperature leads to lower austenite content. Figure 6b shows the calculated temperature distribution during the DSSTTABW process. It can be seen that the temperature of HAZ near the fusion line is higher than 1200 °C, resulting in a lower austenite content as pointed out by Ramirez [24].

3.3 Mechanical properties

3.3.1 Microhardness tests

The microhardness profile from the centerline of DSSTTABW joints to BM is listed in Fig. 7. Three sets of measurements are carried out to ensure the reliability. It is observed that the microhardness of WM is slightly higher than that of BM and HAZ, and the maximum value is 283 $HV_{0.1}$, while the microhardness of HAZ is slightly lower than that of WM and BM, and the minimum value is 253 $HV_{0.1}$. The fluctuation in microhardness values can be attributed to two aspects: microstructure and work-hardening. The existence of more $\gamma 2$ enhances the microhardness of WM [26], while the existence of much coarser ferrite grains decreases the microhardness of HAZ. The work-hardening effect increases the microhardness of WM, while it partially disappears in HAZ.

3.3.2 Transverse tensile tests

Transverse tension tests are carried out for three sets of DSSTTABW joints and one set of the 2205 base metal to analyze the mechanical properties of the DSSTTABW joint, and the results are concluded in Fig. 8. Although all weldments failed on the weld zones, its average
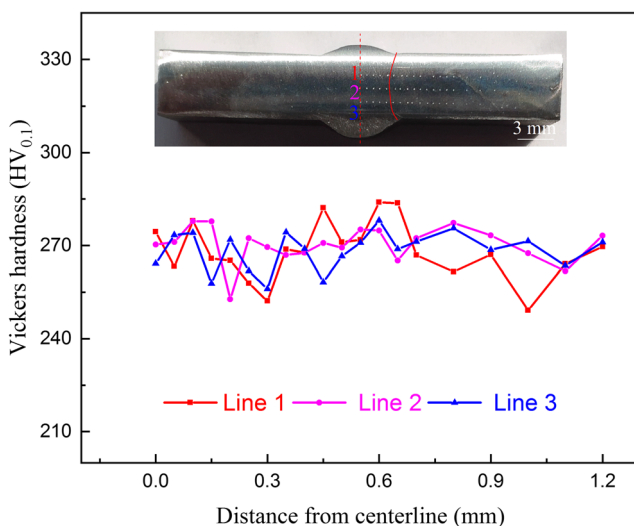
Fig. 7 Microhardness results and the corresponding indentations across the weld. Line 2 locates at the center of the DSSTTABW joint. The distance between line 1 and line 2, and line 2 and line 3 is both 1 mm
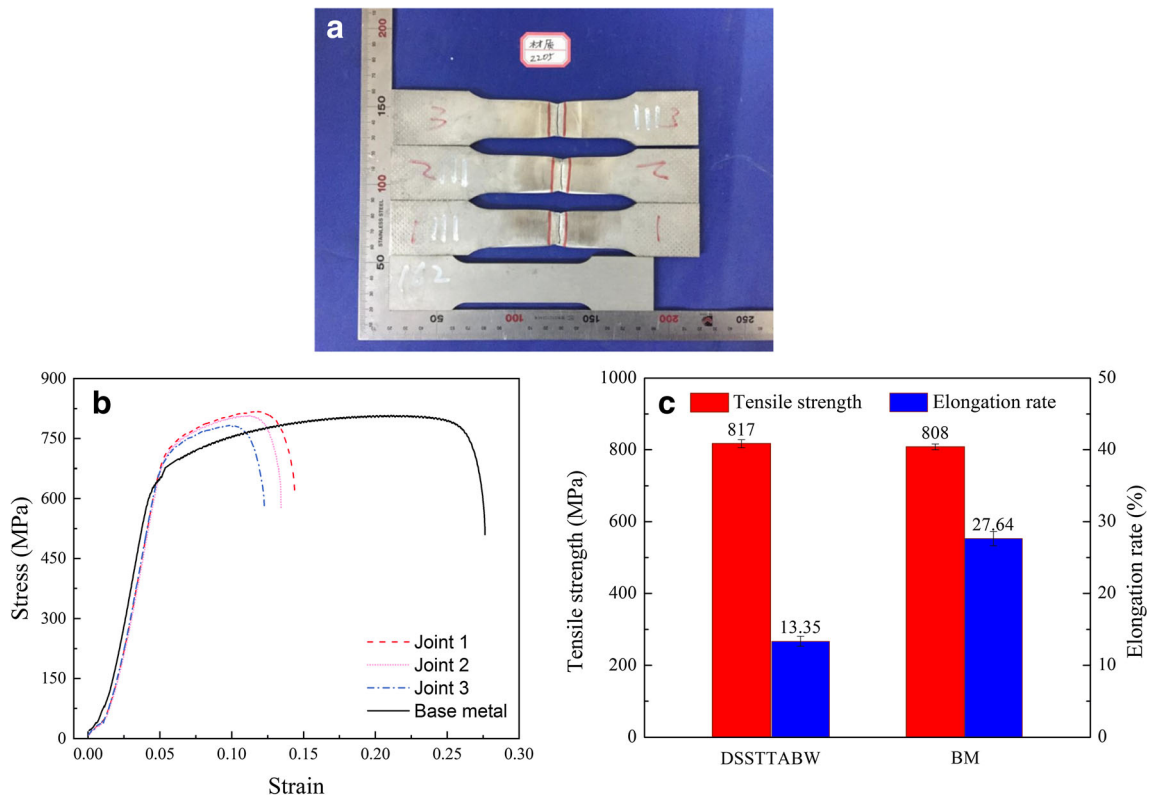
Fig. 8 Macrograph of transverse tensile specimens and tensile strength of the DSSTTABW joints. **a** Macrograph of transverse tensile specimens. **b** The engineering stress-strain curves. **c** Average tensile strength and elongation of DSSTTABW joints and 2205 DSS BM

tensile strength still reaches 817 MPa, which is a little higher than that of 2205 BM (808 MPa), and meets the requirements of engineering application. However, the

elongation of the DSSTTABW joint is much lower than that of the 2205 BM, which is only half of the BM, indicating the reduction of ductility after welding. It

Fig. 9 SEM morphologies of the fracture surface. **a** Low magnification SEM of transverse tensile fracture. **b** The enlargement of square zone B. **c** The enlargement of square zone C in (**a**)
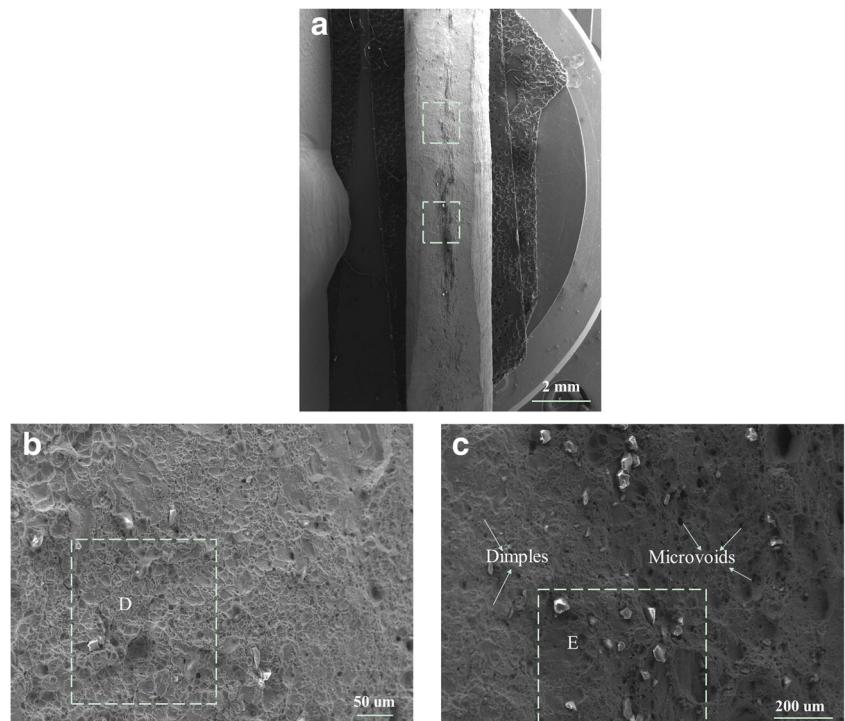
Fig. 10 Element distributions of zone D shown in Fig. 8 obtained by EDS mapping
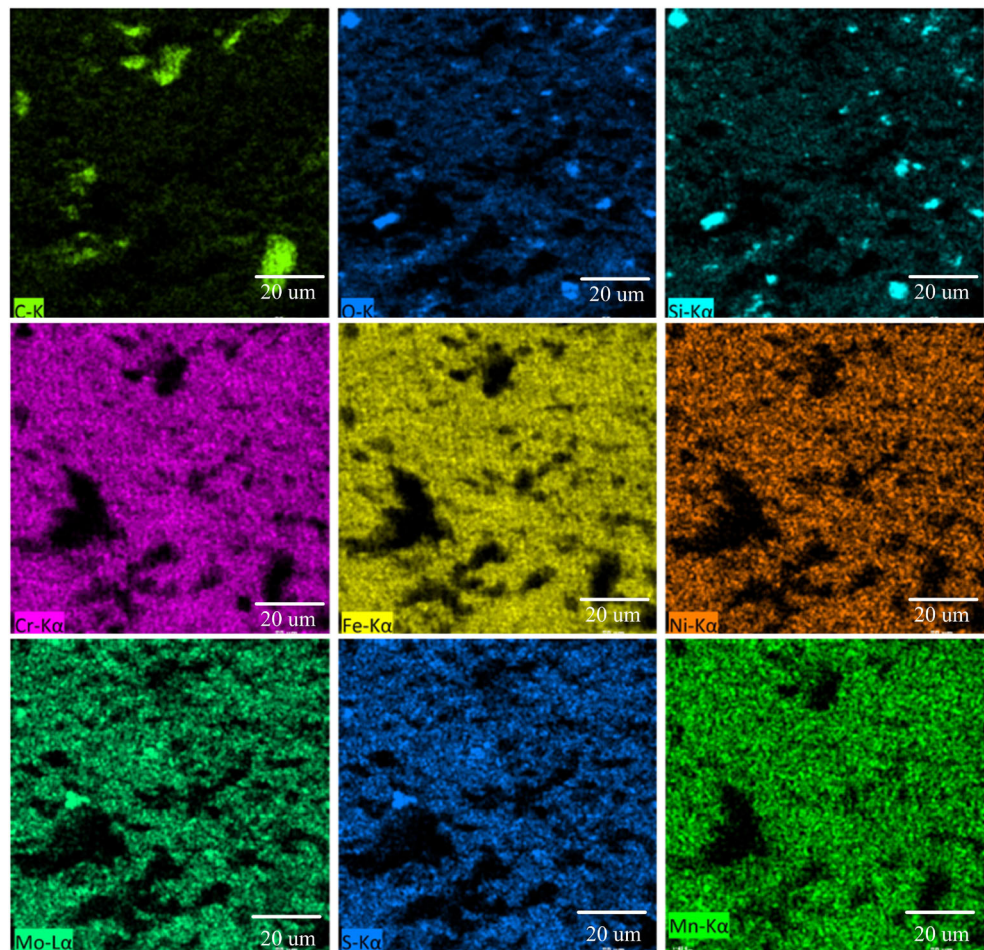
can be attributed that the microstructure of weld metal contains lots of WA with different orientations (as shown in Fig. 4). The cross-distribution of WA hinders the movement of grain boundary, thus increasing the tensile strength. Meanwhile, the existing WA and σ phase in weldments decrease the ductility of DSSTTABW joints.

Figure 9 shows the SEM micrograph for tension fracture of the 2205 DSSTTABW weldment. Technically, the tension fracture for engineering materials can be divided into two kinds of modes: ductile and brittle. A great deal of dimples and microvoids can be found in the micrograph of tension fracture, which indicates the 2205 DSSTTABW joint fracture in the mode of ductile. Meanwhile, lots of inclusions emerge in the weld center of the fracture surface of the DSSTTABW joint. The EDS mapping presents that the inclusions might be SiO_2 or compounds of Si–O–C, as shown in Figs. 10 and 11. There are two reasons accounting for the existence of inter-metallic compounds. Firstly, the lack of protection for weld leads to the generation of intermetallic compound; and secondly, low heat input results in rapid solidification of the weld pool, thus the intermetallic compound left in weld.

3.3.3 Bend tests

Three-point bend tests, including two transverse face bends and two transverse root bends, are carried out to assess the ductility and absence of imperfections on/near the surface of the DSSTTABW joint according to the European Standard ISO 5173. As shown in Fig. 12, four specimens are bended to 180° and no cracks are found. It indicates that the DSSTTABW joint has satisfactory ductility and bending property.

4 Conclusions

In the present study, double-sided synchronous TIP TIG arc butt welding (DSSTTABW) was carried out on the joining of 5-mm-thick SAF 2205 DSSs, and the macrostructure and mi-crostructure characteristics, phase volume fraction, and me-chanical property of DSSTTABW joints, including micro-hardness, transverse tension tests, and bend tests, are analyzed systematically. The main conclusions are drawn as follows:
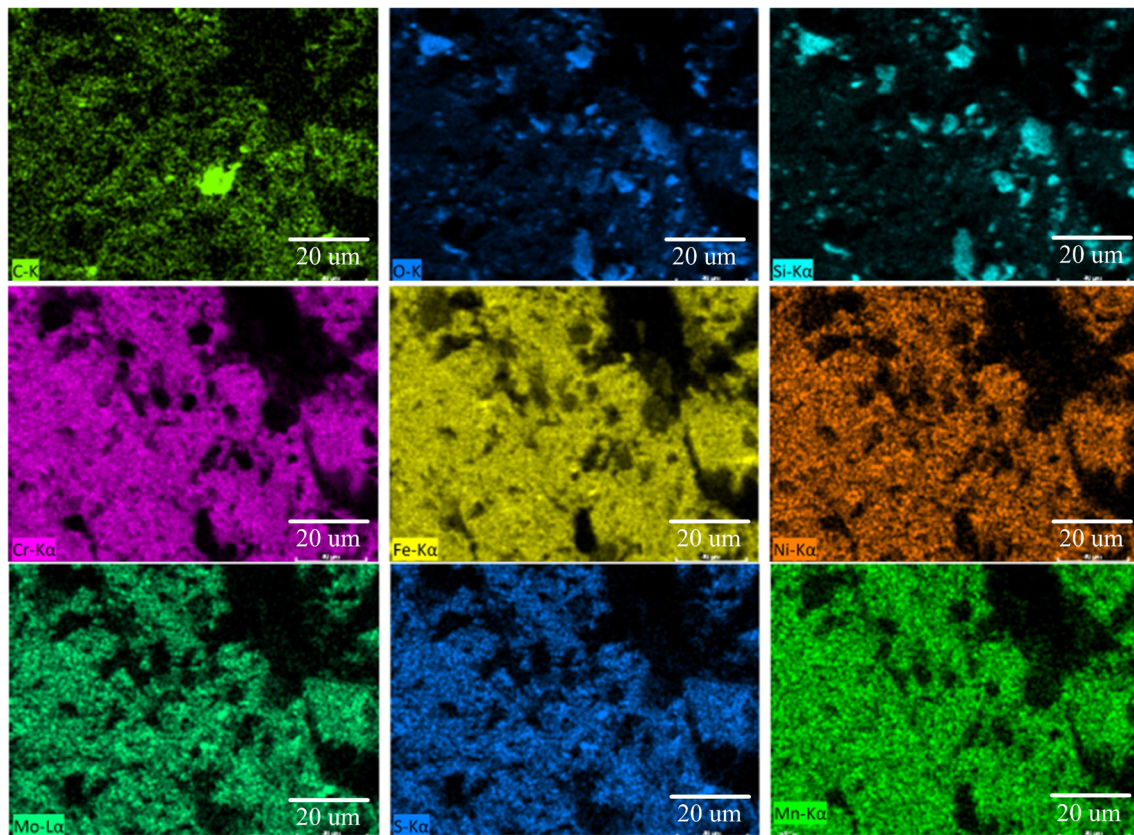
Fig. 11 Element distributions of zone D shown in Fig. 8 obtained by EDS mapping

(1) Sound SAF 2205 DSS double-sided joints (5 mm), with excellent appearance and properties, were obtained through the double-sided synchronous TIP TIG arc butt welding (DSSTTABW) process without grooving.

(2) The WM microstructure of the DSSTTABW joint contains four kinds of austenite phase—GBA, WA, IGA, and γ_2—while the microstructure of HAZ consists of GBA, WA, IGA, and PTA. σ phase exists at the grain boundaries of δ-Fe and austenite of the weld zone through analyses by SEM and EDS. The austenite

fraction in WM of the DSSTTABW joint is 52%, which is slightly higher than the original material (46%) due to the precipitation of γ_2.

(3) The DSSTTABW joints have higher tensile strength and microhardness and lower elongation than 2205 DSS BM. The weldments fracture at the weld zones in the mode of ductile. After bending tests, no surface cracks are observed on the DSSTTABW joint.

Compliance with ethical standards

Conflict of interest   The authors declare that they have no conflict of interest.

References

1. Wang S, Ma Q, Yan L (2011) Characterization of microstructure, mechanical properties and corrosion resistance of dissimilar welded joint between 2205 duplex stainless steel and 16MnR. Mater Des 32(2):831–837
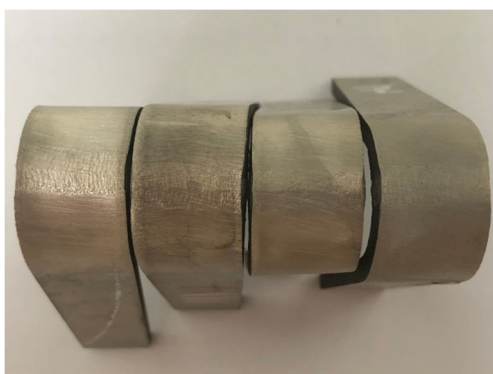
Fig. 12 Macrograph of transverse bend specimens

2. Chern TS, Tseng KH, Tsai HL (2011) Study of the characteristics of duplex stainless steel activated tungsten inert gas welds. Mater Des 32(1):255–263

3. Westin EM, Stelling K, Gumenyuk A (2011) Single-pass laser-GMA hybrid welding of 13.5 mm thick duplex stainless steel. Weld. World. 55(1-2):39–49

4. Esmailzadeh M, Shamanian M, Kermanpur A, Saeid T (2013) Microstructure and mechanical properties of friction stir welded lean duplex stainless steel. Mater Sci Eng A 561:486–491

5. Luo J, Dong Y, Li L, Wang X (2014) Microstructure of 2205 duplex stainless steel joint in submerged arc welding by post weld heat treatment. J Manuf Process 16:144–148

6. Geng S, Sun J, Guo L, Wang H (2015) Evolution of microstructure and corrosion behavior in 2205 duplex stainless steel GTA-welding joint. J Manuf Process 19:32–37

7. Hosseini VA, Bermejo MA, Gårdstam J, Hurtig K, Karlsson L (2016) Influence of multiple thermal cycles on microstructure of heat-affected zone in TIG-welded super duplex stainless steel. Weld World 60(2):233–245

8. Hosseini VA, Hurtig K, Karlsson L (2017) Effect of multipass TIG welding on the corrosion resistance and microstructure of a super duplex stainless steel. Mater Corros 68:405–415

9. Selva BR, Siva SN, Murali KR, Arungalai VS (2018) Studies on the parametric effects of plasma arc welding of 2205 duplex stainless steel. High Temp Mater Processes (Tel Aviv, Israel) 37(3):219–232

10. Zhang YM, Pan C, Male AT (2000) Improved microstructure and properties of 6061 aluminum alloy weldments using a double-sided arc welding process. Metall Mater Trans A 31(10):2537–2543

11. Zhao YB, Lei ZL, Chen YB, Tao W (2011) A comparative study of laser-arc double-sided welding and double-sided arc welding of 6 mm 5A06 aluminium alloy. Mater Des 32(4):2165–2171

12. Qiang W, Wang K (2019) Double-sided coaxial GTA flat-overhead welding of 5083 aluminum alloy. J Mater Process Technol 272:9–16

13. Peng K, Yang C, Lin S, Fan C, Han Y, Wu M (2017) Thermal cycles and its effect on HAZ microstructure and mechanical properties of 10CrNi3MoV steel in double-sided double arc welding. Int J Adv Manuf Technol 93(1-4):967–974

14. Peng K, Yang C, Fan C, Lin S (2018) Microstructure and mechanical properties of simulated unaltered coarse grained heat affected zones of 10CrNi3MoV steel by double-sided double arc welding. J Mater Process Technol 251:225–231

15. Kang P, Yang C, Fan C, Lin S (2018) Thermal processes, microstructure, and mechanical properties near weld toe in double-sided double gas tungsten arc backing welding joint of 10CrNi3MoV steel. Int J Adv Manuf Technol 96(1-4):677–684

16. Zheng Y, Huang J, Wei G, Zhang Y, Zhi C, Chen S, Jian Y (2017) Microstructure and mechanical properties of 5052 aluminum alloy/mild steel butt joint achieved by MIG-TIG double-sided arc welding-brazing. Mater Des 123:69–79

17. Zheng Y, Huang J, Zhi C, Li X, Zhang Y, Chen S, Jian Y (2017) Study on butt joining 5052 aluminum alloy/Q235 mild steel by MIG-TIG double-sided arc welding-brazing process. Weld World 62(1–2):1–10

18. Zhang Y, Huang J, Zhi C, Zheng Y, Hai C, Li P, Chen S (2016) Study on MIG-TIG double-sided arc welding-brazing of aluminum and stainless steel. Mater Lett 172:146–148

19. Qiang W, Wang K (2017) Shielding gas effects on double-sided synchronous autogenous GTA weldability of high nitrogen austenitic stainless steel. J Mater Process Technol 250:169–181

20. Wilson M (2007) TIP TIG : New technology for welding. Ind Robot 34:462–466

21. Xin meng Z , Qing zhu L (2012) Characteristics and prospective application of TIP TIG welding in railway vehicle. Electric Welding Machine 42(9):1–4

22. EN ISO 4136 (2012) Destructive tests on welds in metallic materials. Transverse tensile test

23. EN ISO 5173 (2010) Destructive tests on welds in metallic materials. Bend test

24. Ramirez AJ, Lippold JC, Brandi SD (2003) The relationship between chromium nitride and secondary austenite precipitation in duplex stainless steels. Metall Mater Trans A 34(8):1575–1597

25. Standard N (2004) Welding and inspection of piping. Standards Norway, Lysaker

26. Nowacki J, Lukojc A (2005) Structure and properties of the heat-affected zone of duplex steels welded joints. J Mater Process Technol 164-165:1074–1081